

# High- $p_T$ results from ALICE

M. van Leeuwen<sup>a</sup> *for the ALICE collaboration*

Nikhef, National Institute for Subatomic Physics and Institute for Subatomic Physics of Utrecht University, Utrecht, Netherlands

**Abstract.** We report recent results of high- $p_T$  measurements in Pb–Pb collisions at  $\sqrt{s_{NN}} = 2.76$  TeV by the ALICE experiment and discuss the implications in terms of energy loss of energetic partons in the strongly interaction medium formed in the collisions.

## 1 Introduction

High-energy collisions of heavy nuclei are used to study the high-temperature states of strongly interacting matter and the expected transition from confined matter to a deconfined Quark-Gluon Plasma. Partons with high transverse momentum  $p_T$  are formed in hard scatterings which happen early in the collision. The produced partons then propagate through the hot and dense medium and lose energy through interactions with the medium. Measurements of high- $p_T$  particle production are used to study the interactions between fast partons and the medium and to determine the medium properties using these interactions. Here we report a number of recent high- $p_T$  results from ALICE, the dedicated heavy-ion experiment at the Large Hadron Collider (LHC), from Pb–Pb collisions with a centre-of-mass energy  $\sqrt{s_{NN}} = 2.76$  TeV recorded during the heavy ion run of the LHC in November 2010.

## 2 Nuclear modification factor

One of the most basic measurements that is sensitive to parton energy loss in the hot and dense QCD medium are the charged particle production spectra at high  $p_T$ . The measured transverse momentum spectra of primary charged particles in Pb–Pb collisions with three different centrality selections are shown in the left panel of Fig. 1. The collision centrality is determined using the total multiplicity detected in the forward VZERO detectors and reported as a fraction of the total hadronic cross section, with 0% labeling the most central events. The dashed lines in the Figure indicate a parametrisation of the spectrum measured in pp collisions, scaled by the total number of binary nucleon-nucleon collisions  $\langle N_{coll} \rangle$  as determined from a Glauber model [1, 2]. It can be seen in the figure that for central collisions, the shape of the  $p_T$ -spectra in Pb–Pb collisions is different from pp collisions, with a large suppression for  $p_T = 4 - 10$  GeV/c.

To quantify the differences, the nuclear modification factor

$$R_{AA} = \frac{dN/dp_T|_{PbPb}}{\langle N_{coll} \rangle dN/dp_T|_{pp}},$$

i.e. the ratio between the  $p_T$ -distributions in Pb–Pb collisions  $dN/dp_T|_{PbPb}$  and in pp collisions  $dN/dp_T|_{pp}$ , scaled with the number of binary collisions, is calculated. The nuclear modification factor for charged particles in Pb–Pb collisions with three different centrality selections is shown in the right panel of Fig. 1. The figure clearly shows a significant suppression  $R_{AA} < 1$ . The effect is largest for the most

<sup>a</sup> e-mail: m.vanleeuwen1@uu.nl

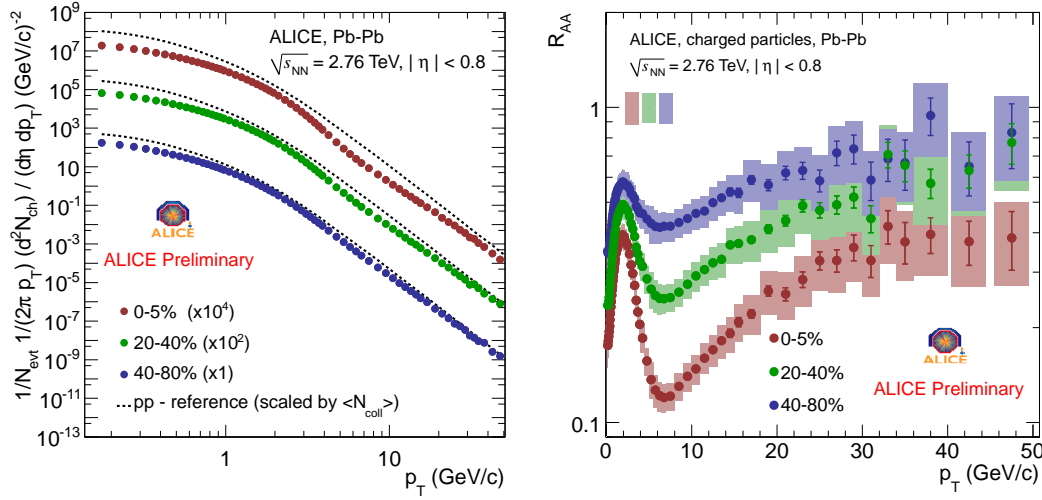


**Fig. 1.** Left panel: Transverse momentum distributions of primary charged particles in Pb–Pb collisions at  $\sqrt{s_{NN}} = 2.76$  TeV with three different centrality selections. Right panel: nuclear modification factor  $R_{AA}$  for charged particles in Pb–Pb collisions at  $\sqrt{s_{NN}} = 2.76$  TeV with three different centrality selections.

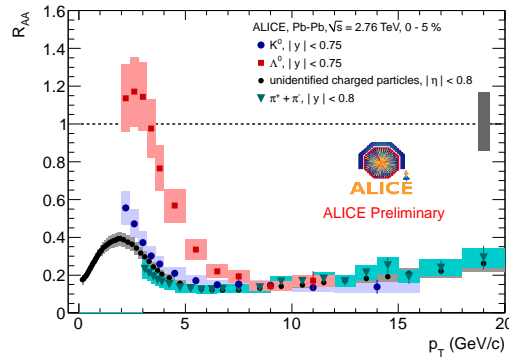
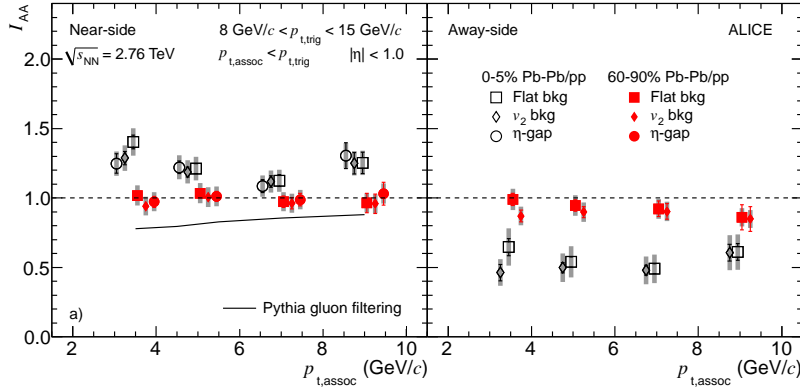


**Fig. 2.** Nuclear modification factor  $R_{AA}$  for identified hadrons in the 0-5% most central Pb–Pb collisions at  $\sqrt{s_{NN}}=2.76$  TeV.

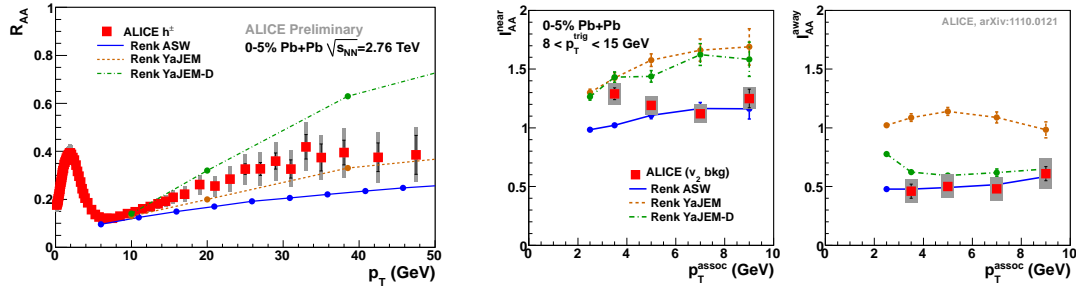
central bin 0 – 5%, where the medium density and the average path length through the medium are the largest. The strongest suppression is seen for  $p_T \approx 7$  GeV/c, with a gradual rise of  $R_{AA}$  towards larger  $p_T$ . The increase of  $R_{AA}$  with  $p_T$  is qualitatively consistent with the expectation that parton energy loss  $\Delta E$  is only weakly dependent on the parton energy  $E$ , leading to a decrease of the relative energy loss  $\Delta E/E$  with increasing  $p_T$ .

Figure 2 shows a comparison of the nuclear modification factor for  $\Lambda$  and  $K_0^s$ , measured using reconstruction of the weak-decay topology, to the result for unidentified charged particles and identified pions for the most central events. It is interesting to see that the  $R_{AA}$  for identified mesons shows a similar  $p_T$ -dependence to the charged particles, while the  $\Lambda$  show much smaller suppression at intermediate  $p_T < 6$  GeV/c. The enhancement of baryon production compared to meson production at intermediate  $p_T$ , might be due to a large contribution of hadron formation by coalescence of quarks from the hot and dense medium [3,4,5].

At higher  $p_T$ , all hadrons show the same suppression, which suggests that the dominant energy loss mechanism is at work at the partonic level. If hadronic energy loss would be important, one would expect to see that different hadrons would have different cross sections for the relevant energy loss mechanism and thus be affected differently.



**Fig. 3.** Ratios of measured charged hadron yield associated with a high- $p_T$  trigger particle with  $8 < p_T < 15$  GeV/c in Pb–Pb and pp collisions on the near ( $|\Delta\phi| < 0.7$ , left panel) and away ( $|\Delta\phi - \pi| < 0.7$ , right panel) sides, as a function of associated particle  $p_T$ . Results are shown for two different centrality selections: peripheral 60-90% (solid red data points) and central 0-5% (open data points). Three different background subtraction methods are shown. The grey bars indicate systematic uncertainties from tracking efficiency and secondary particles [6].



**Fig. 4.** Nuclear modification factor  $R_{AA}$  and per-trigger associated yield modification factor  $I_{AA}$  for the 0-5% most central Pb–Pb collisions compared to model calculations (see text).

### 3 Di-hadron measurements

Using di-hadron correlation techniques, the yield of charged particles produced in association with high- $p_T$  hadrons can be determined. In these measurements, we distinguish the *near-side* yield of particles produced in the same jet as the high- $p_T$  trigger hadron, and the *away-side* or recoil yield of particles in the recoiling jet. This measurement has been performed in pp and Pb–Pb collisions at  $\sqrt{s_{NN}} = 2.76$  TeV using a trigger particle selection of  $8 < p_T^{\text{trig}} < 15$  GeV/c and the ratio  $I_{AA}$  of the associated yield per trigger particle in Pb–Pb and pp collisions is shown in Fig. 3. The results for peripheral collisions (red points in Fig. 3) are very similar to pp ( $I_{AA} \approx 1$ ), while for central collisions (grey points) a slight enhancement of the yield is seen on the near side and a suppression on the away side. Both effects are qualitatively consistent with expectations from parton energy loss in combination with a trigger bias which cause the parton on the away-side to typically have a larger energy loss than the one on the near side. The enhancement on the near side suggests that the trigger particle selects hard scattered partons with higher energy in the Pb–Pb collisions than in pp collisions, due to energy loss of the leading parton.

### 4 Constraining theoretical models

The single-inclusive nuclear modification factor  $R_{AA}$  and the di-hadron modification  $I_{AA}$  sample the geometry of the collision zone with different weights. A simultaneous comparison of both measure-

ments with theoretical calculations can be used to infer the path-length dependence of energy loss [7]. Fig. 4 shows a comparison of the measured  $R_{AA}$  and  $I_{AA}$  to model calculations by Renk [8,9].

The blue line in Figure 4 labeled ‘Renk ASW’ indicates the expected energy loss using the ‘quenching weights’ calculation for the multiple soft scattering approximation by Armesto, Salgado and Wiedemann [10] in a realistic medium-density profile, based on hydrodynamical simulations. One overall scaling parameter was used to relate the local transport coefficient  $\hat{q}$  to the medium density in the hydrodynamical model. This scaling parameter was tuned using measurements from the Relativistic Heavy Ion Collider (RHIC) at  $\sqrt{s_{NN}} = 200$  GeV. The fact that the blue line in the left panel of Fig. 4 is below the measured data points indicates that the single hadron suppression increases less from RHIC to LHC than expected based on the density inferred from multiplicity measurements which are used to tune the hydrodynamical evolution. The agreement of the ASW calculation with the di-hadron correlations is better.

The other two lines in Figure 4 represent energy loss calculations based on a Monte Carlo shower model YaJEM (‘Yet another Jet Energy-loss Model’) [8,9] in which medium-induced radiation is generated by increasing the virtuality as the parton propagates through the medium. Default YaJEM (orange dotted lines in Fig. 4) agrees rather well with the  $R_{AA}$  measurement, while the di-hadron suppression is too weak, due to the approximately linear dependence of the energy loss on the path length  $L$ . YaJEM-D (green dashed lines in Fig. 4) is identical to YaJEM, but introduces a minimum virtuality of the parton  $Q_0 = \sqrt{E/L}$ , related to the requirement that the formation time of each in-medium shower is shorter than its path length through the medium. This causes a stronger path length dependence of the energy loss, similar to the expected  $L^2$  dependence due to the Landau-Pomeranchuk-Migdal effect, which leads to a stronger suppression of the di-hadron recoil yield. However, it should be noted that for the current setting of the model, the inclusive hadron suppression is also smaller ( $R_{AA}$  larger) than measured. Increasing the medium density in YaJEM-D would improve the agreement with the measurements.

All of the models presented in Figure 4 show deviations from the measured values in several places. A more systematic comparison of models with the measurements will be needed to quantify deviations of the models from the data and to disentangle effects from the medium geometry and the path-length dependence of the energy loss process itself.

## 5 Heavy flavour

A specific expectation for radiative parton energy loss is that the effect will be smaller for heavy quarks at lower  $p_T$ , when the quarks travel in the medium at speeds significantly below the speed of light, due to the so-called ‘dead cone’ effect [11,12]. To test this expectation, ALICE has measured the nuclear modification factor of  $D$  mesons, as shown in Fig. 5. The measured  $D$  meson suppression is slightly smaller than the values seen for pions, but the difference is within the current statistical and systematic uncertainties. Related measurements of muon and electron production from heavy flavour decay are reported in [13].

A more precise measurement using a larger data sample and a careful comparison to theoretical expectations are needed to determine whether the dead-cone effect is really observed in experimental data. In addition, measurements of  $B$  mesons are planned, which will have a larger discriminating power, because the dead-cone effect is larger for the heavier  $b$  quarks.

## 6 Jets

Measurements of inclusive hadrons and di-hadrons at high  $p_T$  are mostly sensitive to leading jet fragments, because the steeply falling  $p_T$ -spectrum causes subleading fragments to be overwhelmed by the much larger yields of fragments of lower momentum partons. In addition, the measurements integrate over a large range of energies of the original partons. Jet reconstruction in Pb–Pb collisions has the potential to largely overcome both drawbacks: if the jet cone radius is large compared to the typical

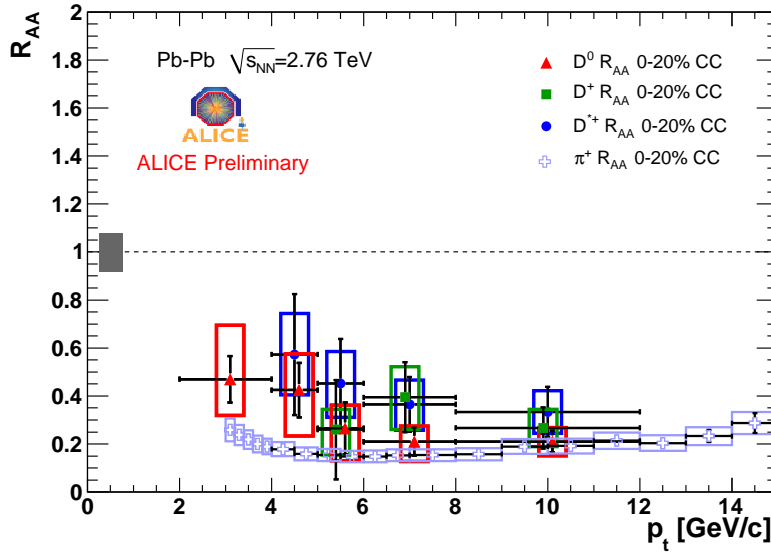


**Fig. 5.**  $R_{AA}$  for  $D$  mesons in 0-20% central Pb-Pb collisions at  $\sqrt{s_{NN}} = 2.76$  TeV. The  $D$  mesons are reconstructed from their hadronic decays:  $D^0 \rightarrow K\pi$ ,  $D^\pm \rightarrow K\pi\pi$  and  $D^{*\pm} \rightarrow \pi^\pm + D^0 \rightarrow \pi^\pm + K\pi$ .

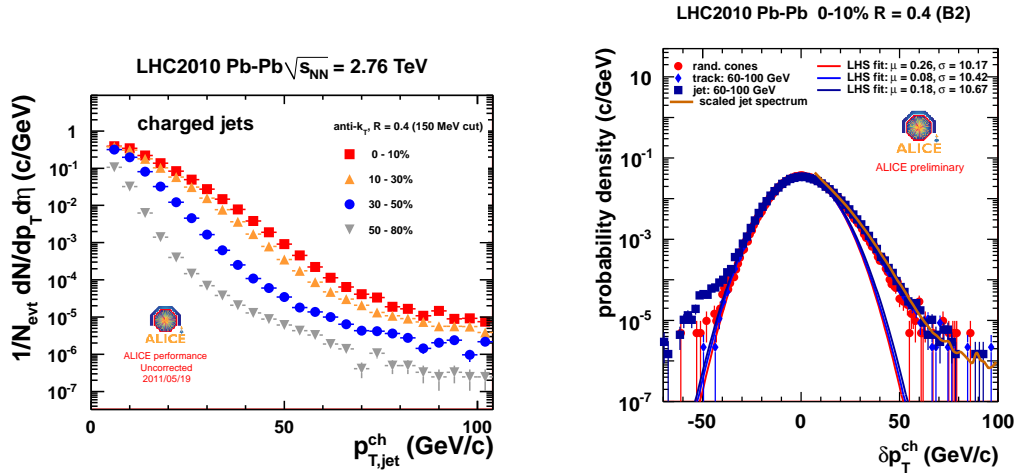


**Fig. 6.** Left panel: Transverse momentum distributions of reconstructed jet spectra in Pb-Pb collisions with different centralities, using only charged particle tracks. The energy of the uncorrelated background has been subtracted, but no corrections are applied for background fluctuations and detector effects. Right panel: Background energy distribution in central 0-10% events, determined using random cones and jet and track embedding. The curves show Gaussian fits to the left-hand side (LHS) of the distributions.

angles of gluon emission, most the radiated energy is recovered by the jet-finding algorithm, which then provides a measure of the energy of the parton from the hard scattering (before energy loss).

However, jet reconstruction in Pb-Pb collisions at the LHC is challenging, due to the large underlying event energy. The left panel of Fig. 6 shows the reconstructed momentum distribution of charged jets from the anti- $k_T$  algorithm with  $R = 0.4$ , after subtraction of the uncorrelated background, which is measured on event-by-event basis using the  $k_T$  algorithm from the FastJet package [14]. At low  $p_T$ , a clear excess is visible in the jet spectrum of central events compared to peripheral events due

to background fluctuations, which lead to ‘fake jets’. Judging from the curvature of the jet spectrum, fluctuations/fake jets dominate the jet spectrum up to  $p_T \approx 70$  GeV/ $c$  for central (0-10%) events.

The right panel of Fig. 6 shows the background fluctuations as measured directly using random cones and two types of embedding [15]. The random cone technique places ‘jet’ cones in the event at random location and then calculates the background-subtracted transverse momentum in the cone to measure the fluctuations. The embedding technique adds a track or several tracks from a jet to the event and then compares the reconstructed transverse momentum to the transverse momentum of the input track or jet to measure the fluctuations. The three methods give very similar results, indicating that the background measurement is mostly sensitive to the track density (and correlations) in the event and not to details of the jet fragmentation or the placement of the cone.

The jet results can only be interpreted in conjunction with the background fluctuation measurement. ALICE is currently pursuing unfolding techniques to remove the effect of the background fluctuations from the reconstructed jet spectrum. Given the large  $p_T$ -reach of the fluctuations, a larger data set is likely needed to extend the measured jet spectrum and allow unfolding of the background fluctuations.

## 7 Outlook

In these proceedings, we have reported first results on high- $p_T$  measurements of Pb–Pb collisions at  $\sqrt{s_{NN}} = 2.76$  TeV performed by ALICE. The effects of the energy loss of partons propagating through the hot and dense medium are clearly seen in the suppression the inclusive yields of charged particles and di-hadrons, as well as for heavy mesons.

The goal of this research is to develop a quantitative understanding of the interactions between energetic partons and the medium and to use this understanding to determine properties of the medium such as the energy density or transport coefficient(s). A careful comparison of multiple measurements with theoretical expectations is needed to develop our understanding of parton energy loss. A first attempt of such a comparison for the LHC energy was shown in Fig. 4, but a more systematic approach will be pursued in the near future.

The results in these proceedings are based on the data sample of about 20M hadronic interactions collected in the heavy ion run of the LHC in 2010. A much larger data sample has been collected in November 2011, which will allow to improve the precision of the heavy flavour and jet measurements and extend the  $p_T$ -range over which the various measurements can be performed. These improvements will be essential to further constrain the theory of parton energy loss.

## References

1. M.L. Miller, K. Reygers, S.J. Sanders, P. Steinberg, *Ann.Rev.Nucl.Part.Sci.* **57**, 205 (2007), [nucl-ex/0701025](#)
2. K. Aamodt et al. (ALICE Collaboration), *Phys.Rev.Lett.* **106**, 032301 (2011), [1012.1657](#)
3. Z.W. Lin, C.M. Ko, *Phys. Rev. Lett.* **89**, 202302 (2002), [nucl-th/0207014](#)
4. R.C. Hwa, C.B. Yang, *Phys. Rev.* **C67**, 034902 (2003), [nucl-th/0211010](#)
5. R.J. Fries, B. Muller, C. Nonaka, S.A. Bass, *Phys. Rev. Lett.* **90**, 202303 (2003), [nucl-th/0301087](#)
6. K. Aamodt et al. (ALICE) (2011), [1110.0121](#)
7. T. Renk, *Phys.Rev.* **C76**, 064905 (2007), [0708.4319](#)
8. T. Renk, K.J. Eskola, *Phys.Rev.* **C84**, 054913 (2011), [1106.1740](#)
9. T. Renk, H. Holopainen, R. Paatelainen, K.J. Eskola, *Phys.Rev.* **C84**, 014906 (2011), [1103.5308](#)
10. C.A. Salgado, U.A. Wiedemann, *Phys.Rev.* **D68**, 014008 (2003), [hep-ph/0302184](#)
11. Y.L. Dokshitzer, D. Kharzeev, *Phys.Lett.* **B519**, 199 (2001), [hep-ph/0106202](#)
12. N. Armesto, C.A. Salgado, U.A. Wiedemann, *Phys.Rev.* **D69**, 114003 (2004), [hep-ph/0312106](#)
13. C. Suire (ALICE) (2012), these proceedings
14. M. Cacciari, G.P. Salam, G. Soyez (2011), [1111.6097](#)
15. B. Abelev et al. (ALICE) (2012), [1201.2423](#)